Stretching, Packing, and Thermodynamics in Highly Branched Polymer Melts

Rashmi Patil and Kenneth S. Schweizer*

Department of Materials Science and Engineering, University of Illinois, 1304 W. Green Street, Urbana, Illinois 61801

Tsun-Mei Chang

Department of Chemistry, University of Wisconsin-Parkside, 900 Wood Road, Kenosha, Wisconsin 53141-2000

Received October 25, 2002

ABSTRACT: Within the framework of the polymer reference interaction site model (PRISM) theory, we formulate a simplified method for enforcing conformational self-consistency associated with screening of intrapolymer excluded-volume interactions. It is built on a utilization of the Flory ideality concept, preaveraging of site inequivalency, and the insensitivity of equation-of-state properties of chemically identical polymers to global architecture variation at constant temperature and pressure. The approach allows calculation of the influence of chain branching on average macromolecular stretching under meltlike conditions. Nonideal conformational swelling, intermolecular pair correlation functions, and the cohesive energy as a function of architectural variables have been studied for a variety of star and regular comb models. Predictions for a specific highly globular comb melt are in good agreement with a recent experiment. The relatively weak influence of the nonuniversal local aspect ratio and melt compressibility on polymer stretching is also established. Implications for the χ parameter in isotopic star or comb blends, and the miscibility of mixtures of linear and branched polymers, are briefly discussed.

I. Introduction

An important factor influencing polymer material properties is global architecture. Branching generally results in large modifications relative to linear chain systems for properties such as melt rheology, diffusion, and percent crystallinity.[1] Blending chemically identical linear and branched polymers can lead to enhanced or new properties[2] and has recently been the subject of fundamental physical studies.[3−6] A primary consequence of branching is intramolecular crowding, which results in nonideal conformational stretching to reduce unfavorable excluded-volume interactions. For systems such as grafted polymer brushes, sterically stabilized colloids, and diblock copolymers, self-consistent-field theory and scaling approaches have been useful for predicting conformational nonidealities.[7] The long wavelength incompressibility constraint generally plays a central role in capturing the coarse-grained consequences of monomer level excluded-volume forces. In polymer solutions, density fluctuations must be taken into account, and field theories and blob scaling ideas have been developed.[8,9] These approaches assume the relevant "mesh" length scale is large compared to local chemical lengths and hence are restricted to semidilute solutions.

Even in dense one-component melts or concentrated solutions significant conformational nonidealities may be present for heavily branched polymers. A microscopic theoretical approach is required to treat this problem. The polymer reference interaction site model (PRISM) theory has been widely applied to self-consistently predict intramolecular and intermolecular correlations for linear chain polymers at high concentrations.[10] The most advanced version is a hybrid method which couples single-chain Monte Carlo simulation with PRISM theory for the many-chain problem.[10−14] Heavily branched polymers present additional technical complexities such as strong site inequivalency. Grayce and Schweizer[15] developed a self-consistent PRISM theory to treat concentrated solutions and dense melts of 4−12-arm stars. A multiple region core−corona model was constructed, and their predictions are in semiquantitative agreement with the limited SANS experiments available.[16,17] Generalization of this approach to combs, even if regularly branched, is more difficult, and the computational expense can rapidly grow.

The goal of the present paper is to formulate a conceptually simple and easy to implement theory within the PRISM framework for conformational nonideality in branched polymer melts. The simplifications proposed are motivated by elementary screening ideas and experimental equation-of-state behavior. An equivalent site preaveraging approximation is introduced which restricts discussion of conformational properties to the global radius of gyration or an averaged statistical segment length. The latter is what are generally accessible in neutron scattering experiments unless partial labeling methods are employed. The theory is applied to a variety of star and regular comb polymer melts, and comparisons with prior fully self-consistent PRISM results for stars[10,15] are performed to test its accuracy. Applications to highly globular combs are compared to recent scattering experiments.[3] The influence of branching on the melt cohesive energy is also investigated. An additional motivation for the present work is to provide a foundation to treat blends of architecturally distinct polymers. Reliable prediction of enthalpic contributions to miscibility requires knowledge of local intermolecular correlations, which are generally very sensitive to nonideal conformational perturbations.

* Corresponding author: e-mail kschweiz@uiuc.edu.

10.1021/ma021624n CCC: $25.00
Published on Web 03/11/2003

The remainder of the paper is structured as follows. Section II summarizes PRISM theory and the polymer models employed. Our simplified screening approaches are formulated in section III. Model calculations for star melt conformational properties are given in section IV. Results for polymer swelling, intermolecular pair correlations, the static structure factor, and the cohesive energy of star and comb melts are presented in section V. Section VI applies the theory to a specific highly globular, "soft colloid" like comb polymer and makes comparisons with a recent experiment. The paper concludes in section VII with a brief summary and discussion.

II. PRISM Theory and Polymer Models

A. Theory. PRISM theory is a polymeric generalization the reference interaction site model theory of Chandler and Andersen[18] for small rigid molecular fluids. In-depth reviews are available.[10,18] For a homopolymer melt, ignoring site inequivalency effects, the so-called PRISM equation in Fourier space (wavevector k) is given by[10]

$$\hat{h}(k) = \hat{\omega}(k)\,\hat{C}(k)\,\hat{\omega}(k) + \rho\hat{\omega}(k)\,\hat{C}(k)\,\hat{h}(k) \qquad (1)$$

Here ρ is the site (monomer) number density, $h(r) \equiv g(r) - 1$, where $g(r)$ is the site−site intermolecular pair correlation function, $C(r)$ is the site−site intermolecular direct correlation function, and the single polymer structure factor is given by

$$\hat{\omega}(k) = \frac{1}{N}\sum_{i}^{N}\sum_{j}^{N}\hat{\omega}_{ij}(k) \qquad (2)$$

$\hat{\omega}_{ij}(k)$ is the Fourier transform of the intramolecular probability distribution function between sites i and j on the same polymer, and N is the degree of polymerization. The dimensionless structure factor describing collective density fluctuations is

$$\hat{S}(k) = \hat{\omega}(k) + \rho\hat{h}(k) \qquad (3)$$

To solve the PRISM equation, a closure approximation which relates h, ω ,C, and the intermolecular pair potential is required. For dense, hard-core molecular and polymeric fluids a rather accurate approximation is the site−site Percus−Yevick (PY) approximation[10,18]

$$g(r) = 0, \quad r < d$$
$$C(r) \approx 0, \quad r > d \qquad (4)$$

where d is the hard-core diameter of a site. The PRISM integral equation is solved numerically using the standard Picard algorithm.[19]

For flexible polymers, $\hat{\omega}(k)$ should be, in principle, determined in a self-consistent manner with the intermolecular correlations. As a first approximation, one can bypass this difficult task in dense melts by invoking the Flory idea that chains are ideal.[8,9] In the applications described in this work, we adopt this simple approach for linear chains. However, even at fixed monomer chemistry the complete screening concept underlying the Flory ideality idea will be less accurate for branched polymers. Our goal is to *predict* the modification of macromolecular dimensions upon branching with the linear chain architecture serving as the "reference state".

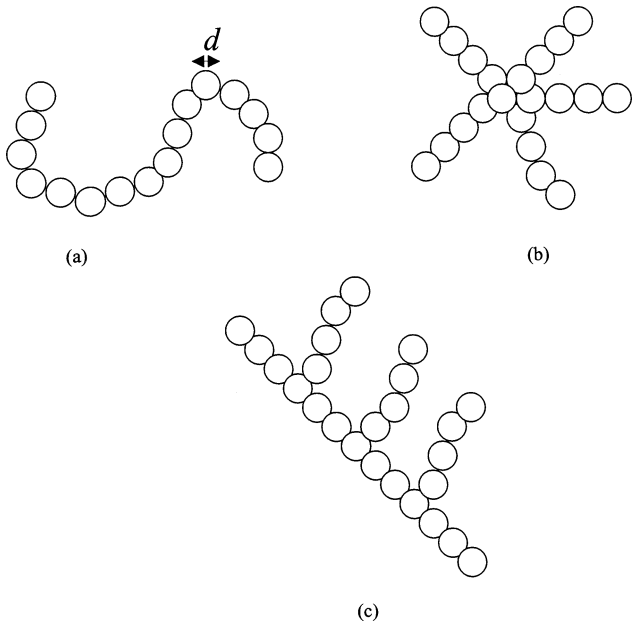

Figure 1. Model chain (a), star (b), and comb (c) polymers, where d is the hard-core diameter of a site. The linear chain is characterized by the number of segments N_{ch}, the star by the number of segments per arm N_a and number of arms f, and a regular comb by the number of segments in backbone N_{bb}, number of segments per branch N_c, and the number of branches f_c.

B. Polymer Models and Thermodynamic Properties. In this initial study the single polymer structure factors (Figure 1) are described by a coarse-grained Gaussian model for which analytic results are well-known. For a linear chain[9] with a statistical segment length σ_{ch} and degree of polymerization N_{ch}

$$\hat{\omega}(k) = \frac{1}{(1-y)^2}\left[(1-y^2) - \frac{2y(1-y^{N_{ch}})}{N_{ch}}\right] \qquad (5)$$

where $y = \exp(-k^2\sigma_{ch}^2/6)$ and the radius of gyration $R_g^2 = (N_{ch}^2 - 1)\sigma_{ch}^2/6N_{ch}$. For a star polymer[20] with f arms and N_a monomers per arm

$$\hat{\omega}_s(k) = \{fN_a(1-y^2) - 2yf(1-y^{N_a}) - fy^2(1-y^{N_a})^2 + [fy(1-y^{N_a}) + 1 - y]^2\}/[(1-y)^2(fN_a+1)] \qquad (6)$$

with radius of gyration

$$R_{g,st} = \frac{\sigma}{\sqrt{6}(N_a f + 1)}(2f\,N_a + 3f^2N_a^{\,2} - 2f\,N_a^{\,3} + 3f^2N_a^{\,3})^{1/2} \qquad (7)$$

$R_{g,st}$ increases as the arm length or arm number increases, and the large arm number limit is $\sqrt{3}$ times larger than the R_g of one arm. For a regularly branched comb polymer of N_{bb} backbone segments and f_c side chains composed of N_c segments[20]

$$\hat{\omega}_c(k) = \frac{1}{(1-y)^2(N_{bb}+f_cN_c)} \times \left\{ N_{bb}(1-y^2) - 2y(1-y^{N_{bb}}) + f_c[N_c(1-y^2) - 2y(1-y^{N_c})] + \{2y^{M_b+2}(1-y^{N_c})^2(f_c - 1 - f_c y^{M_b} + y^{f_cM_b})\}/(1-y^{M_b})^2 + 2y(1-y^{N_c})\left[f_c(1+y) - \frac{2y^{M_b/2}(1-y^{f_cM_b})}{(1-y^{M_b})} \right] \right\} \quad (8)$$

where $M_b \equiv (N_{bb}+1)/f_c$. The radius of gyration is

$$R_{g,co} = \frac{\sigma}{\sqrt{12}(N_{bb}+f_cN_c)}[-8f_cN_c - 12f_cN_c^2 + 6f_c^2 - 4f_cN_c^3 + 6f_c^2N_c^3 + M_b(4f_c - 2f_cN_c^2 + 6f_c^2N_c^2 + 2f_c^3N_c^2) + M_b^2(-6f_c^2 - f_cN_c + 4f_c^3N_c) + 2f_c^3M_b^3]^{1/2} \quad (9)$$

In general, $R_{g,co}$ increases with branch length or number, with the dependence on the latter being much weaker than on branch length. Comb architectures will be indicated by the notation $N_{bb} - f_c - N_c$.

A coil volume fraction, ϕ_{poly}, is defined to quantify the internal density of polymers of variable global architecture. For a polymer of total degree of polymerization N_s, with a site hard-core volume of $\pi d^3/6$, enclosed in a spherical region of radius R_g, one has

$$\phi_{poly} = \frac{N_s}{8}\left(\frac{d}{R_g}\right)^3 \quad (10)$$

As the degree of branching increases, the polymer becomes more compact and coil density increases. Our primary interest is melt structure where the repulsive excluded-volume interactions are dominant. However, it also is of interest to determine how branching changes the cohesive energy which is sensitive to local interpolymer contacts. For this purpose a site−site Lennard-Jones-like attraction is employed:[10]

$$U(r) = \epsilon\left[\left(\frac{d}{r}\right)^{12} - 2\left(\frac{d}{r}\right)^6\right], \quad r \geq d \quad (11)$$

The cohesive energy is computed in the standard "high-temperature approximation" appropriate for dense melts where the structural correlations are those of the athermal reference system

$$U_{coh} = -\rho\int d\vec{r}\; U(r)\, g(r) = \delta^2 \quad (12)$$

where δ is a dimensionless solubility parameter.[21,22]

All melts are characterized by a normalized segment length or aspect ratio $\Gamma = \sigma/d$, reduced density ρd^3, and dimensionless compressibility $S_0 = \rho k_B T \kappa_T$. For flexible polymers[21] such as polyolefins or polydienes $\Gamma \sim 1-1.5$. We select $\Gamma = 1$ and 1.4, which are representative of polymers such as polyethylethylene (PEE) and polyethylene (PE), respectively.[21,23] The experimental melt values of $S_0 \sim 0.04-0.3$ for $T \sim 200-450$ K.[24]

III. Nonideal Conformational Behavior

The rigorous self-consistent treatment of conformation within PRISM theory proceeds from calculation of a pair decomposable medium-induced solvation potential between pairs of sites on the same polymer.[10,25] The solution of the corresponding nonlocal effective single polymer conformational statistics problem can be achieved either approximately or via Monte Carlo simulation. On the basis of the PY style approach, the solvation (or screening) pair potential, $W(r)$, is given by[11,12,15]

$$w(r) = -\int d\vec{r}' \int d\vec{r}''\; C(\vec{r} - \vec{r}')\, \rho S(\vec{r}' - \vec{r}'')\, C(\vec{r}'') \quad (13)$$

$$\beta W(r) = -\ln(1 + w(r)) \quad (14)$$

Our goal is to bypass rigorous implementation of self-consistency since our primary interest is the pure architecture effect, i.e., comparing linear and branched polymers of fixed chemical structure. Under the latter condition, at constant temperature and pressure the melt density is nearly independent of global macromolecular architecture.[3,24] Such insensitivity is expected for other thermodynamic properties, such as the isothermal compressibility or its dimensionless analogue S_0, although we are unaware of specific measurements. The physical reason for this expectation is the short spatial range of collective density fluctuations in dense liquids. We exploit this fact to formulate three closely related ideas for solving the screening problem of branched polymers which we refer to as methods A, B, and C.

A. Constant S_0 Criterion. First, the statistical segment length σ_{ch} of the linear polymer of interest is specified in eq 5. The Flory ideality idea asserts that the intermolecular and intramolecular excluded-volume effects effectively cancel such that the conformation of a single-chain molecule can be described by ideal Gaussian statistics. This idea is implemented by varying the reduced density of the linear chain melt such that the calculated segment−segment second virial coefficient vanishes[9,12]

$$v_0 = \int_0^\infty d\vec{r}\; (1 - e^{-\beta(U_0(r)+W)}) \to 0 \quad (15)$$

where U_0 is the bare intramolecular segment−segment pair potential taken here to be of the hard-sphere form. At this density the medium-induced solvation potential and intramolecular repulsive interactions are exactly balanced in an average sense at the segmental level. Typically, the result of this constraint is $\rho d^3 \sim 2$, a reasonable value representative of polyethylene based on a site being a CH_2 group.[10] Knowledge of the linear polymer reduced density fixes the theoretical S_0 value, which in our present studies is typically ~0.03−0.06 depending on the chain aspect ratio. *The branched polymer of interest is then considered (using eqs 6 or 8) at exactly the same reduced density but allowed to swell to give the same dimensionless compressibility.* Hence, the effective statistical segment length of the branched polymer, σ_{br}, is predicted and is different than its chain analogue. This procedure corresponds to a constant compressibility, or dimensionless density fluctuation amplitude, constraint within a "full screening" model for the chain.

B. Complete Screening Criterion. The only difference from approach A is σ_{br} is also determined via the condition $v_0 \equiv 0$. The two methods give essentially the same results in all the diverse cases we have

studied. This can be qualitatively understood from combining eqs 14 and 15 to yield

$$\rho v_0 = \frac{4\pi}{3}\rho d^3 + 4\pi\rho\int_d^\infty \mathrm{d}r\, r^2 w(r) \approx \frac{4\pi}{3}\rho d^3 + \rho^2\hat{C}(0)^2\,\hat{S}(0) = \frac{4\pi}{3}\rho d^3 - \frac{1}{S_0} \quad (16)$$

The approximate equality follows from taking $d \to 0$ in the lower limit of the integral, and the last equality is exact for $N \gg 1$.Hence, the constant S_0 suggests constant v_0.

C. S_0 Constraint Criterion. Another small variant of approach A is to compute the reduced density of a polymer chain melt with selected σ_{ch} to reproduce an a priori chosen value of dimensionless compressibility S_0. As before, the branched polymer melt density is chosen to be identical, and σ_{branch} is varied to get the same dimensionless compressibility. This approach does not literally enforce Flory ideality in the sense of a vanishing second virial coefficient. However, in practice, we find for experimentally relevant values of S_0 the computed values of v_0 are extremely small relative to the bare hard-core value.

Our motivation for considering multiple schemes is threefold. First, it allows the robustness of our predictions to approximation details to be established. Second, contact with prior, far more sophisticated self-consistent PRISM studies for star polymers[15] can be made. Third, methods A and C are only useful for homopolymer melts, but method B can be employed to predict conformational nonidealities in multicomponent blends and block copolymers. To facilitate comparison with prior work, *screening model C is used in all presented results unless stated otherwise.*

IV. Swelling in Star Polymer Melts

In this section we study the nonideal conformational properties of dense star polymer melts over a wide range of values of dimensionless melt compressibility, number of arms f, and arm length N_a. Figure 2 shows R_g^2 (in units of d^2) as a function of $f = 4-32$. Note that for $f >$ 12 a dendritic core is generally required,[5] a practical aspect we do not take into account. The dimensionless compressibility was fixed at $S_0 = 0.05$, a realistic value primarily chosen to allow comparison with the calculations of ref 15.

Interesting power law dependences of R_g^2 on f are found with effective exponents that decrease with increasing arm length due to the reduced internal coil density. The power law behavior for 100 unit arm stars is in remarkably good agreement with the study by Grayce and Schweizer (GS),[10,15] who employed PRISM theory and a full numerical self-consistent treatment of the screening problem within a multisite core−corona description (and for which $S_0 \sim 0.05$ at a meltlike packing fraction of 0.55). For $N_a = 100$ stars with $f =$ 4−12, GS obtained $R_g^2 \sim f^{0.38}$, compared to $R_g^2 \sim f^{0.37}$ from our much simpler approach. Quantitative comparisons are given in Table 1. The trends are nearly identical. This level of agreement is encouraging regarding the utility of our far simpler approach to accurately reproduce the relative trends of the more sophisticated PRISM theory. Of course, it does not establish the absolute accuracy since PRISM is an approximate theory and there are no relevant computer simulations to compare with. The precise numerical

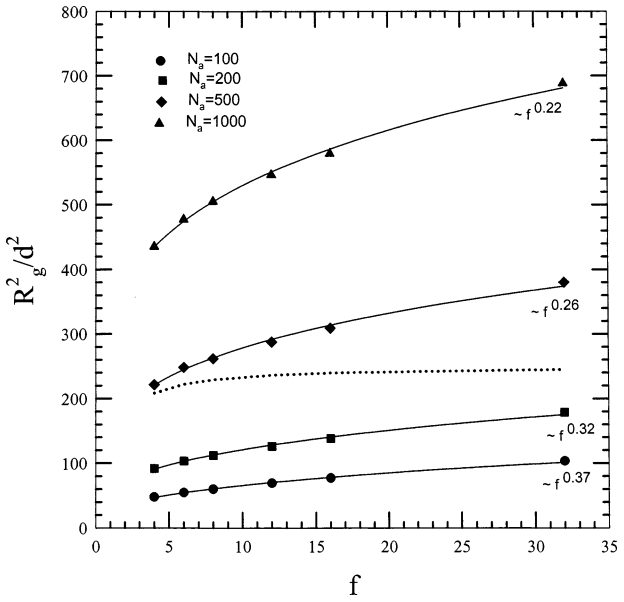

Figure 2. Mean-square radius of gyration (in units of d^2) of star melts as a function of arm number f based on screening model C for $N_a = 100$ (circles), 200 (squares), 500 (diamonds), and 1000 (triangles). The curves are power law fits with the effective exponents indicated. The dashed line is R_g^2 for $N_a =$ 500 if the star polymer is not allowed to stretch.

Table 1. Comparison of the Squared Radius of Gyration R_g^2 (in Units of d^2) for $N_a = 100$ Star Melts Obtained Using Screening Model C and $S_0 = 0.05$ with Prior Fully Self-Consistent PRISM Theory Calculations Based on a Core−Corona Star Model[15]

f	R_g^2 ($S_0 = 0.05$)	R_g^2 (ref 15)	$R_g^2/[R_g^2(f=4)]$	$R_g^2/[R_g^2(f=4)]$ (ref 15)
4	47.7	70.3	1.00	1.00
6	54.7	83.0	1.15	1.18
8	60.1	91.0	1.26	1.29
12	69.1	106	1.45	1.51

values of R_g^2 are roughly 30% smaller than the results of GS. This is due to the neglect of explicit local stiffness which was included in ref 15 by using a semiflexible discrete Koyama chain model.[10,15]

The dashed line in Figure 2 is an example of the literally ideal Gaussian behavior if stretching is ignored. As seen from Table 2, the sensitivity of the scaling exponent of R_g^2 to the nonuniversal chain aspect ratio and dimensionless compressibility is remarkably weak.

R_g^2 as a function of arm length N_a has been studied over the range $N_a = 100-1000$ and $f = 4-32$ (not plotted). At low arm number ($f = 4$, 6) the radius of gyration squared varies almost linearly with N_a, corresponding to ideal behavior. At larger f its growth with arm length becomes slower, $R_g^2 \sim N_a^x$, where $x = 0.89$ ($f = 12$) and 0.82 ($f = 32$) corresponding to an effectively more compact object.

Another quantity that characterizes the nonideal conformational differences between stars and linear chains having the *same total number of sites* is the so-called "g-factor" defined as the ratio $g = (R_g/R_{g,ch})^2 < 1$. Figure 3 shows results for various arm degrees of polymerization as a function of arm number all at fixed $S_0 = 0.05$. This quantity decreases in a power law fashion as N_a is increased, with an apparent exponent that weakly increases with arm length. We also find (not shown) that g is far more sensitive to arm number than arm length: $g \sim N_a^{-y}$ with y increasing from 0.04 ($f =$ 4) to 0.17 ($f = 32$) for $N_a = 100-1000$. For the $f = 4-12$

Table 2. Effective Scaling Exponents of the Star Melt Conformational Properties σ_{st}, R_g^2, and g defined as $\sigma_{st} \sim f^a$, $R_g^2 \sim f^b$, and $g \sim f^c$ *

	$S_0 = 0.05$			$S_0 = 0.25$		
N_a	a	b	c	a	b	c
100	0.15 (0.13)	0.37 (0.34)	−0.63 (−0.65)	0.15 (0.14)	0.38 (0.35)	−0.62 (−0.65)
200	0.13 (0.11)	0.32 (0.29)	−0.68 (−0.71)	0.12 (0.11)	0.33 (0.30)	−0.67 (−0.70)
500	0.09 (0.08)	0.26 (0.23)	−0.74 (−0.77)	0.09 (0.08)	0.26 (0.24)	−0.77 (−0.76)
1000	0.08 (0.06)	0.22 (0.2)	−0.78 (−0.80)	0.07 (0.06)	0.23 (0.20)	−0.84 (−0.80)

* Screening model C is employed. Results are given for various arm lengths, two compressibility conditions, and $\sigma_{ch} = 1.0$ (1.4).

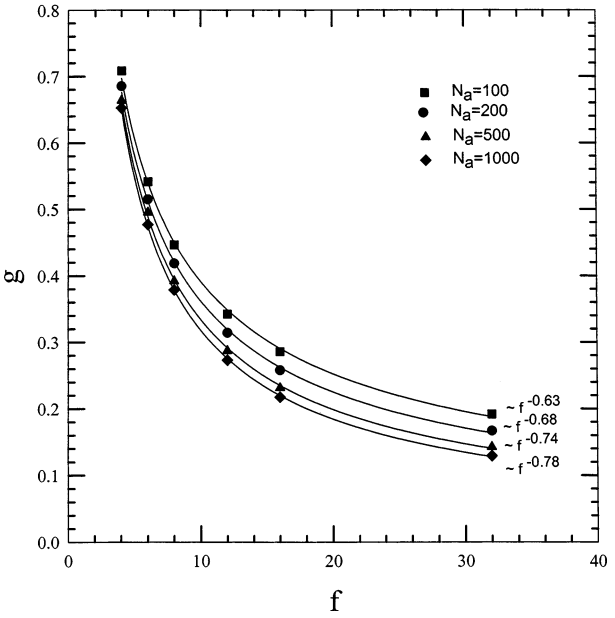

Figure 3. Ratio of the star to chain radius of gyration squared at fixed total degree of polymerization as a function of arm number for $N_a = 100$ (squares), 200 (circles), 500 (triangles), and 1000 (diamonds). The curves are power law fits with the effective scaling exponents indicated.

and $N_a = 100$ case we find $y \sim -0.05$, compared to $y \sim -0.04$ of GS.[15] By construction, our star model is a linear chain at $f = 2$, and the curves in Figure 3 smoothly go to $g \rightarrow 1$.

Table 2 gives the apparent exponents in the power law dependences of σ_{st} and g with f for various arm lengths, $\sigma_{ch} = 1.0$ and $\sigma_{ch} = 1.4$, and two values of compressibility $S_0 = 0.05$ and 0.25 which span the typical experimental range. When $N_a = 100$, the exponent for the power law behavior of g is ~ -0.625, while the far more sophisticated calculation of GS[15] found an exponent of -0.64. The scaling exponents for σ_{st} and g are remarkably insensitive to the dimensionless compressibility and chain aspect ratio, again suggesting nearly universal behavior as found for the radius of gyration. As the arm length is increased by a factor of 10, the segment length (g-factor) scaling exponent changes by a factor ~ 2 ($\sim 20\%$), in a nearly local aspect ratio and compressibility independent manner. Hence, to a good approximation, the nonideal swelling behavior as characterized by effective scaling exponents depends only on polymer architecture.

V. Packing Correlations, Swelling, and Cohesive Energy in Star and Comb Melts

In this section we present results for intermolecular site−site pair correlations. Although the polymer model is a coarse-grained one, the calculated $g(r)$'s are directly relevant to computer simulations of "tangent bead" type models, which hopefully can be simulated in the near future. Also, as discussed at length in ref 21, the intermolecular packing for such models actually can be surprising similar to far less coarse grained and atomistic models.

Results for the real-space structure of star melts are given in Figure 4a−c for $N_a = 100$ and various arm numbers. The linear chain analogue with $N_{ch} = N_a$ is shown for comparison. The ratio of star statistical segment length to its chain analogue (indicated by the quantity σ), the polymer volume fraction ϕ_{poly}, and the star cohesive energy normalized by its chain analogue, U, are also listed. An example of the influence of the nonuniversal bare aspect ratio and melt compressibility is revealed by comparing parts a−c of Figure 4. All the pair correlation functions display a correlation hole which becomes more pronounced with increasing number of arms, compressibility, and/or decreasing bare aspect ratio. The local solvation shell oscillations are increasingly suppressed as melt compressibility (aspect ratio) is increased (decreased). These trends all follow from the reduced degree of polymer interpenetration and intermolecular contacts associated with a growing polymer internal volume fraction which increases by a factor of ~ 3 as $f = 4 \rightarrow 32$.

The quantities σ, ϕ_{poly}, and U also show systematic trends. The degree of star swelling varies by $\sim 20\%$ with bare statistical segment length σ_{ch}. Reductions of $\sim 10-30\%$ of the star normalized cohesive energy occur as arm number increases, which are largest for the less compressible and/or lower bare aspect ratio polymer melts.

An example of the consequences of increasing the arm and chain length to 1000 on packing and other properties is shown in Figure 5. The more open nature of these polymers results in less stretching and cohesion differences, but all the qualitative trends relative to the chain polymer are the same as in Figure 4.

Figure 6a−c shows the analogous set of results as in Figure 4 for three different regular comb architectures with $N_{ch} = 999 = N_{bb}$. All combs have the same number of total sites and are highly branched in the sense that the side chain mass is 10 times larger than the backbone mass. These calculations highlight the role of arm length and number on intermolecular packing at fixed comb molecular weight. The basic trend is that as the number (length) of side chains increases (decreases), intermolecular contacts are reduced. As expected, the comb polymer packs most similarly to a linear polymer when there are a small number of long branches, as is relevant to linear low-density polyethylene (LLDPE).[1,2] As the number of branches increases, the degree of swelling, cohesive energy, and intermolecular correlations of comb melts deviate significantly from the linear polymer behavior. The dependence on compressibility S_0 and chain statistical segment length σ_{ch} is qualitatively the same as found for stars.

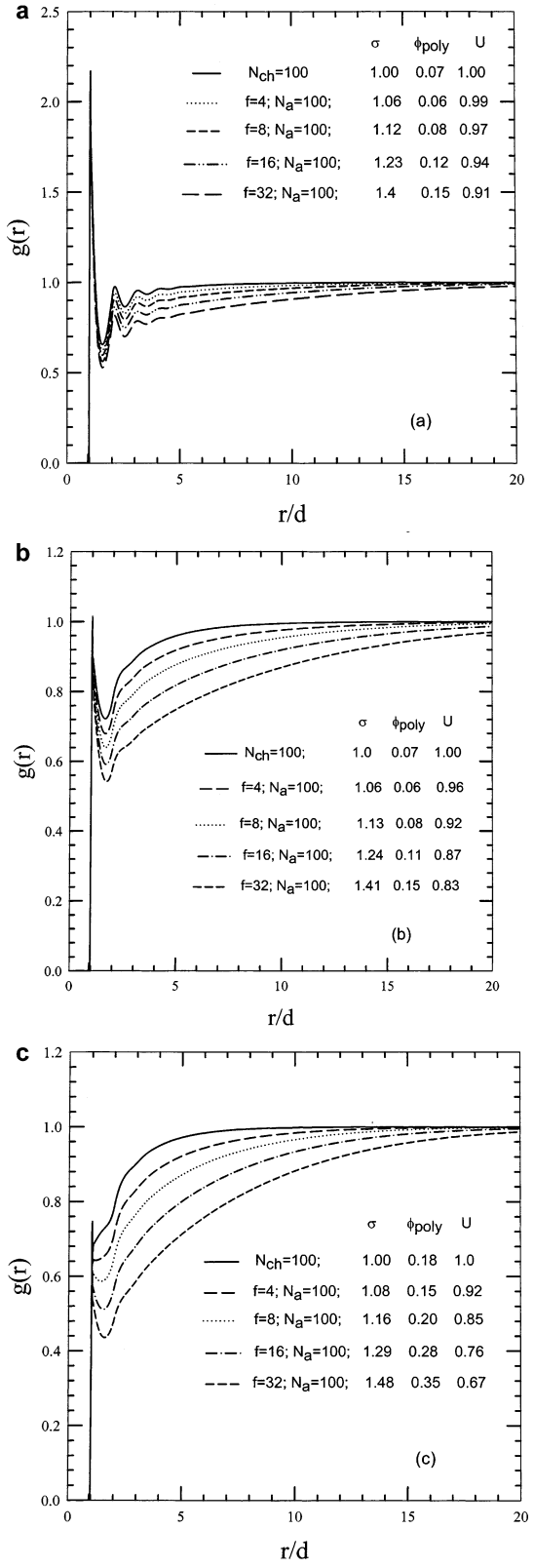

Figure 4. Intermolecular site−site pair correlation functions for a linear polymer of $N_{ch} = 100$ and star polymers of $N_a = 100$ and $f = 4$, 8, 16, and 32 for (a) $S_0 = 0.05$, $\sigma_{ch} = 1.4$, (b) $S_0 = 0.25$, $\sigma_{ch} = 1.4$, and (c) $S_0 = 0.25$, $\sigma_{ch} = 1.0$. The ratio of the star polymer statistical segment length to its chain polymer analogue, σ, the corresponding cohesive energy ratio, U, and the coil volume fraction ϕ_{poly} are tabulated.

The screening approach C corresponds to identical values of the dimensionless compressibility S_0 (a $k = 0$ thermodynamic property) for linear and branched polymers. An interesting question is to what extent do fluctuations on finite length scales, as quantified by $S(k)$, depend on branching. Representative answers to this question are given in Figure 7 for linear, star, and highly branched combs with $\sigma_{ch} = 1.0$ and $S_0 = 0.25$. Modest differences are present in the wide-angle amorphous halo region. The inset shows the influence of nonuniversal variables ($\sigma_{ch} = 1.4$, $S_0 = 0.05$). Remarkably, all the scattering profiles are nearly identical when $S_0 = 0.05$. If $\sigma_{ch} = 1.4$ and $S_0 = 0.25$ (not shown), the results are nearly the same as in the inset. Hence, the insensitivity is enhanced with increasing bare local aspect ratio. The basic conclusion from Figure 7 is that identical collective fluid structure on all length scales is nearly realized in different architecture melts by enforcing the constant S_0 constraint (or approaches A or B). Whether this level of insensitivity is changed if more realistic polymer models are employed is an open question requiring future study. However, such an insensitivity is consistent with the idea that melt thermodynamic properties are not sensitive to global architecture.

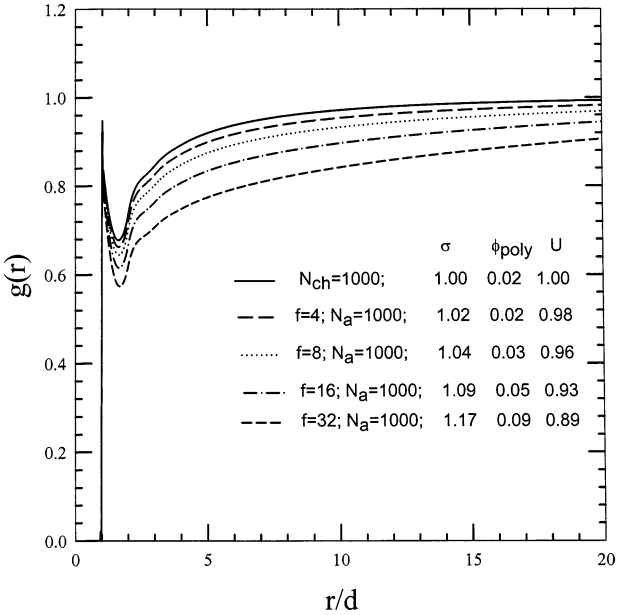

Figure 5. Intermolecular pair correlation function for a linear polymer of $N_{ch} = 1000$ and $\sigma_{ch} = 1.4$, and star polymer melts with $N_a = 1000$ and $f = 4$, 8, 16, and 32, all at a fixed $S_0 = 0.25$. σ, ϕ_{poly}, and U have the same meaning as in Figure 4.

VI. Globular Combs

Chen et al.[3] recently synthesized a globular, "soft colloid" like comb polymer of polyethylethylene (PEE). It consists of $N_{bb} = 183$ backbone monomers, and $f_c \sim 54$ randomly placed side chains of $N_c = 253$ monomers. We study the corresponding two regularly branched comb models with $f_c = 46$ and 61 and compare with a $N_{ch} = 1009$ linear polymer melt also relevant to the experiments.

All three screening approaches A, B, and C have been implemented for $\sigma_{ch} = 1.0$ and 1.4. For method C intramolecular repulsions are not completely screened, but the computed chain and comb segmental second virial coefficients are found to be only ~1% of the bare excluded volume. The $v_0 = 0$ complete screening approach (not shown) yields a corresponding S_0 for the comb melt which is ~99% of the compressibility found from approach A. This again demonstrates the near

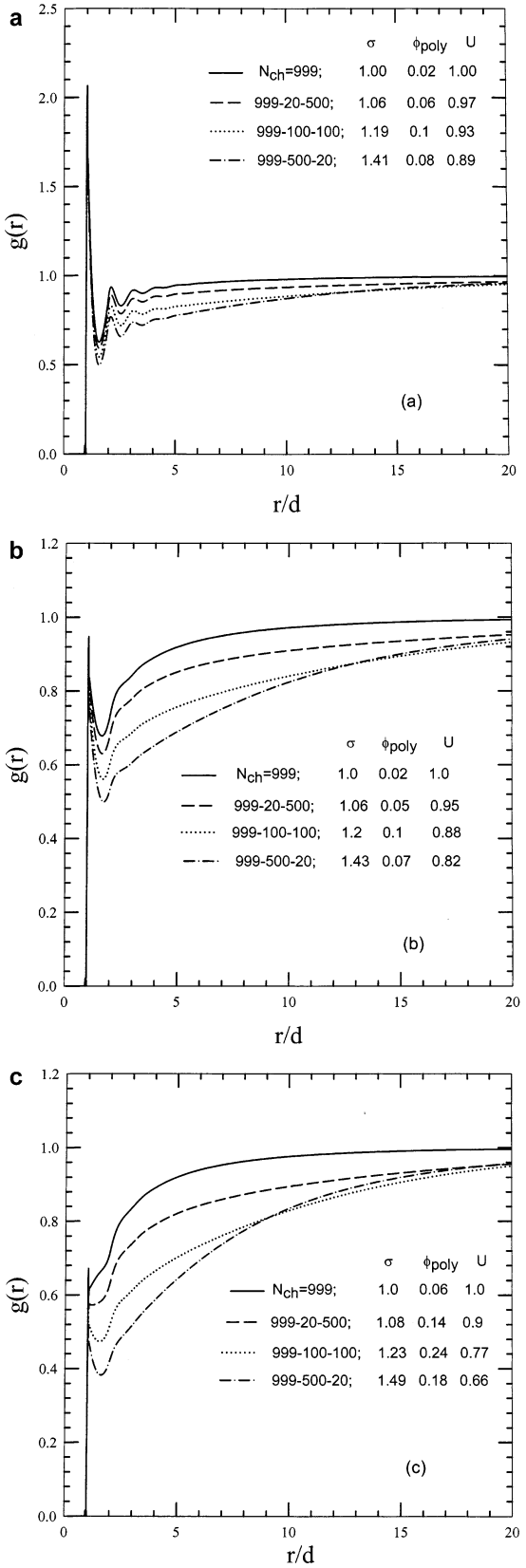

Figure 6. Intermolecular site−site pair correlation functions for a linear polymer of $N_{ch} = 999$ and three comb polymers of different branching architectures all having the same total number of segments and (a) $S_0 = 0.05$, $\sigma_{ch} = 1.4$, (b) $S_0 = 0.25$, $\sigma_{ch} = 1.4$, and (c) $S_0 = 0.25$, $\sigma_{ch} = 1.0$.

insensitivity of our predictions to which specific screening idea is employed even for very highly branched polymers.

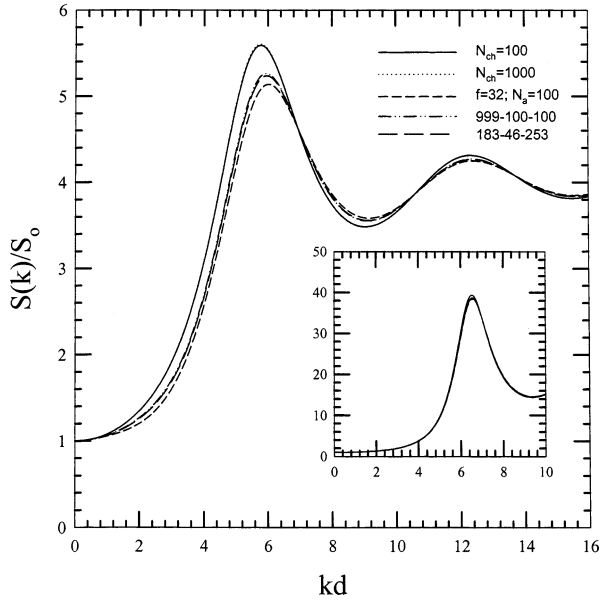

Figure 7. Structure factor normalized by its value at $k = 0$ for various linear, star, and comb polymer melts. Here $\sigma_{ch} = 1.0$ and $S_0 = 0.25$. The inset shows the same quantity for $\sigma_{ch} = 1.4$ and $S_0 = 0.05$.

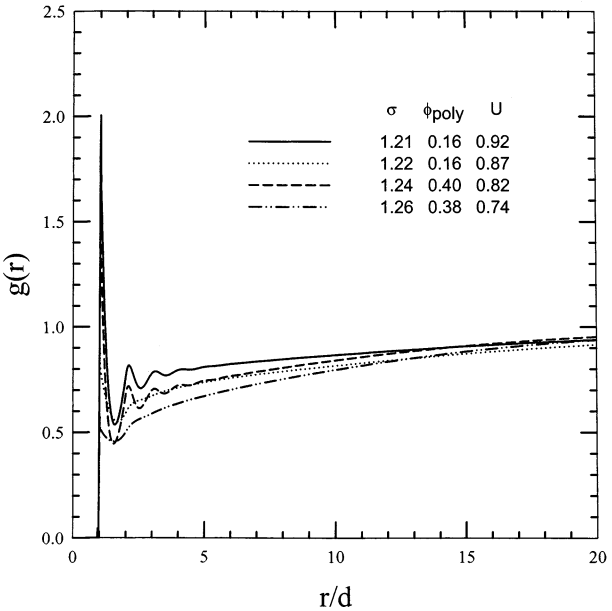

Figure 8. Intermolecular pair correlation function for a globular comb polymer melt having $N_{bb} = 183$ backbone segments, and $f_c = 46$ side chains each with $N_c = 253$ segments. The solid and dotted lines represent the screening approach A and $S_0 = 0.25$ constraint method C, respectively, for $\sigma_{ch} = 1.4$. The dashed line and dashed−dotted lines are the same cases when $\sigma_{ch} = 1.0$.

Figure 8 shows results for $f_c = 46$. The trends in the radial distribution functions regarding the influences of compressibility and aspect ratio are qualitatively similar to those presented in Figure 6. Significant swelling is predicted, and for $\sigma_{ch} = 1$ the comb cohesive energy is ∼78% of its linear counterpart. For the locally more expanded case corresponding to $\sigma_{ch} = 1.4$ the comb can interpenetrate and pack more efficiently, resulting in enhanced intermolecular contacts and a relative cohesive energy of ∼90%. Table 3 summarizes results for swelling and cohesive energy ratios for the different screening schemes, two values of σ_{ch}, and $f_c = 46$ and 61.The more functionalized ($f_c = 61$) and locally flexible

Table 3. $\sigma_{comb}/\sigma_{ch}$ Effective Segment Length Ratio for Chains of $N_{ch} = 1009$ and a 183−f_c−253 Comb Model[a]

	$\sigma_{ch} = 1.0$			$\sigma_{ch} = 1.4$		
f_c	A	B	C	A	B	C
46	1.242 (0.824)	1.244 (0.83)	1.262 (0.743)	1.211 (0.919)	1.212 (0.919)	1.221 (0.866)
61	1.302 (0.798)	1.305 (0.804)	1.326 (0.705)	1.265 (0.907)	1.267 (0.908)	1.278 (0.846)

[a] Results for $f_c = 46$ and 61 are given for each of the three screening models A, B, and C (with $S_0 = 0.25$). The corresponding values of the cohesive energy ratio U_{comb}/U_{ch} are indicated in the parentheses.

($\sigma_{ch} = 1$) comb is modestly more swollen, but this is not a large effect. For a locally branched monomer like PEE[21] $\sigma_{ch} \approx d$, and swelling of 25−35% relative to the chain polymer is predicted. This value is in good agreement with recent small-angle neutron scattering experiments[3] which find a segment swelling ratio of $\sim 1.3 \pm 0.15$.

The reduction in intermolecular contacts due to branching must have consequences on the χ parameter in isotopic blends. For structurally symmetric isotopic blends χ is proportional to the cohesive energy[8,26,27]

$$\chi_{iso} \propto (\lambda - 1)^2 \beta U_{coh} \tag{17}$$

where $\lambda \approx 1.01$ is due to polarizability differences (van der Waals attraction) upon deuteration.[26] Though this form follows from Flory−Huggins theory, $g(r)$ contains an architecture-dependent local correlation hole. The ratio of chain to comb isotopic χ parameter equals the corresponding cohesive energy ratio, U, given in Table 3. For a $\sigma_{ch} = d$ PEE-like model, a reduction of χ_{iso} by $\sim$20−30% is predicted. This is qualitatively consistent with experiments[3] which found smaller values of χ_{iso} for the isotopic comb blend than its linear chain analogue.

VII. Summary and Conclusions

Within the PRISM theory framework a simple approach to enforcing conformational "self-consistency" or screening in branched polymers has been formulated and applied. The method employs an elementary realization of the Flory ideality concept, preaveraging of connectivity-related monomer inequivalency, and the idea that the melt density and isothermal compressibility of chemically identical polymers are (to a good first approximation) independent of macromolecular architecture. Since compressible PRISM theory can predict the connection between polymer conformation, packing, and thermodynamics, nonuniversal aspects associated with local chemical structure can be studied. For the Gaussian polymer model, the latter are just the local bare aspect ratio and the dimensionless isothermal compressibility. The approach can be generalized to semiflexible models with explicit stiffness and other more realistic polymer models.[10] This will allow assessment of the sensitivity of results to including more local and nonideal aspects of branched polymer intramolecular structure. The latter issue has been recently addressed for branched polymers in dilute solutions.[28]

Nonideal conformational predictions for star melts were compared with far more sophisticated (and rigorous) self-consistent PRISM studies,[15] and excellent agreement was found. New model calculations were performed of conformational properties, interchain correlations, and collective density fluctuations for a range of star arm numbers and lengths and values of compressibility and local aspect ratio that span the typical range in dense melts. Regularly branched combs were also studied, with an emphasis on highly branched architectures which show enhanced swelling with increasing number of branches at fixed total side chain molecular weight. Results for a globular PEE comb melt are consistent with a recent experiment,[3] although many more experimental tests are needed.

The present melt work sets the stage for studying binary architectural blends of chains and branched polymers. The role of nonlocal entropic vs local enthalpic contributions to χ can be explored and compared to recent experiments.[3−6] The question of whether the enthalpic and entropic contributions are independent, and the role of global architecture and conformational asymmetry,[20,29,30] can be addressed as will be reported elsewhere.[31]

Acknowledgment. Helpful and simulating discussions and correspondence with F. S. Bates and M. D. Foster are gratefully acknowledged. Financial support is from the Department of Energy, Division of Materials Science, via Oak Ridge National Laboratory in cooperation with the UIUC Frederick Seitz Materials Research Laboratory.

References and Notes

(1) Sperling, L. H. *Introduction to Physical Polymer Science*, 2nd ed.; John Wiley & Sons: New York, 1992.
(2) Utracki, L. A. *Polymer Alloys and Blends*; Hanser Publishers: Munich, 1989.
(3) Chen, Y. Y.; Lodge, T. P.; Bates, F. S. *J. Polym. Sci., Part B: Polym. Phys.* **2000**, *38*, 2965.
(4) Chen, Y. Y.; Lodge, T. P.; Bates, F. S. *J. Polym. Sci., Part B: Polym. Phys.* **2002**, *40*, 466.
(5) Greenberg, C. C.; Foster, M. D.; Turner, C. M.; Corona-Galvan, S.; Cloutet, E.; Quirk, R. P.; Butler, P. D.; Hawker, C. *J. Polym. Sci., Polym. Phys.* **2001**, *39*, 2549.
(6) Martter, T. D.; Foster, M. D.; Yoo, T.; Xu, S.; Lizzaraga, G.; Quirk, R. P.; Butler, P. D. *Macromolecules* **2002**, *35*, 9763.
(7) Halperin, A.; Tirrell, M.; Lodge, T. P. *Adv. Polym. Sci.* **1991**, *100*, 31.
(8) de Gennes, P.-G. *Scaling Concepts in Polymer Physics*; Cornell University Press: Ithaca, NY, 1979.
(9) Doi, M.; Edwards, S. F. *The Theory of Polymer Dynamics*; Oxford Science Publications: Oxford, 1986.
(10) Schweizer, K. S.; Curro, J. G. *Adv. Chem. Phys.* **1997**, *98*, 1.
(11) Grayce, C. J.; Schweizer, K. S. *J. Chem. Phys.* **1994**, *80*, 6846.
(12) Grayce, C. J.; Yethiraj, A.; Schweizer, K. S. *J. Chem. Phys.* **1994**, *100*, 6857.
(13) Melenkevitz, J.; Schweizer, K. S.; Curro, J. G. *Macromolecules* **1993**, *26*, 5571.
(14) Puetz, M.; Curro, J. G.; Grest, G. S. *J. Chem. Phys.* **2001**, *114*, 2847.
(15) Grayce, C. J.; Schweizer, K. S. *Macromolecules* **1995**, *28*, 7461.
(16) Horton, J. C.; Squires, G. L.; Boothroyd, A. T.; Fetters, L. J.; Rennie, A. R.; Glinka, C. J.; Robinson, R. A. *Macromolecules* **1989**, *22*, 681. Lantman, C. W.; MacKnoght, W. J.; Rennie, A. R.; Tassin, J. F.; Monnerie, L.; Fetters, L. J. *Macromolecules* **1991**, *24*, 2810.
(17) Hutchings, L. R.; Richards, R. W. *Macromolecules* **1999**, *32*, 880.
(18) Chandler, D.; Andersen, H. C. *J. Chem. Phys.* **1972**, *57*, 1930. Chandler, D. In *Studies in Statistical Mechanics*; Montroll, E., Lebowitz, J., Eds.; North-Holland: Amsterdam, 1982; Vol. 8, p 274.
(19) Hansen, J. P.; McDonald, I. R. *Theory of Simple Liquids*, 2nd ed.; Academic Press: New York, 1986.
(20) Fredrickson, G. H.; Liu, A. J.; Bates, F. S. *Macromolecules* **1994**, *27*, 2503.
(21) Schweizer, K. S.; David, E. F.; Singh, C.; Curro, J. G.; Rajasekaran, J. J. *Macromolecules* **1995**, *28*, 1528.
(22) Hildebrand, J. H.; Scott, R. L. *The Solubility of Non-Electrolytes*, 3rd ed.; Dover: New York, 1964.

(23) Fetters, L. J.; Lohse, D. J.; Richter, D.; Witten, T. A.; Zirkel, A. *Macromolecules* **1994**, *27*, 4639.
(24) Zoller, P.; Walsh, D. *Standard Pressure−Volume−Temperature Data for Polymers*; Technomic Publishers: Lancaster, 1995.
(25) Chandler, D.; Singh, Y.; Richardson, D. M. *J. Chem. Phys.* **1984**, *81*, 1975.
(26) Bates, F. S.; Wignall, G. D.; Koehler, W. *Phys. Rev. Lett.* **1985**, *55*, 2425. Bates, F. S.; Wignall, G. D. *Phys. Rev. Lett.* **1986**, *57*, 1429.
(27) Schweizer, K. S. *Macromolecules* **1993**, *26*, 6050.
(28) See, for example: Timushenko, E. G.; Kuznetsov, Y. A.; Connolly, R. *J. Chem. Phys.* **2002**, *116*, 3905.
(29) Singh, C.; Schweizer, K. S. *J. Chem. Phys.* **1995**, *103*, 5814.
(30) Singh, C.; Schweizer, K. S. *Macromolecules* **1997**, *30*, 1490.
(31) Patil, R.; Schweizer, K. S.; Chang, T. M. *J. Polym. Sci., Polym. Phys.*, to be submitted.

MA021624N